ADVANCED MATERIALS INTERFACES

www.advmatinterfaces.de

Flexible Wire-Shaped Perovskite Photodetector via Joule Heating for Improved Crystallization and Performance

*Geoffrey Ryan Adams, Nirmal Adhikari, Helen Parker, and Okenwa Okoli**

Organolead triiodide perovskite ($CH_3NH_3PbI_3$) is used extensively as the absorber material for both solar cells and photodetectors; however, the reported photodetectors are all planar and flexible planar devices. To the best of knowledge the first flexible wire-shaped perovskite photodetector is reported. The performance of the wire-shaped perovskite photodetector on carbon nanotube yarn (CNY) critically depends on the surface geometry and annealing conditions. The use of joule heating method for uniform control of temperature on CNY surface results in smooth perovskite crystalline films, which are used to produce self-powering photodetectors with strong responsivity (10.2 A W^{-1}), detectivity (1.76×10^{11} J), and I_{light}/I_{dark} (45). This development displays the role of joule heating in the annealing process and demonstrates a cheap, repeatable method for the fabrication of self-powered perovskite photodetectors.

1. Introduction

Semiconducting behavior has been observed for over a century and a half, with the first integration of the p–n junction photodetector attributed to Weckler in 1965.[1] Since then, photodetectors have been fabricated with a variety of materials including GaN, ZnO, Si, InGaAs, quantum dots, carbon nanotubes, and polymers.[1a,2] Now with perovskite on the scene, we have another material showing similar performance, but lower fabrication cost through large-scale role to role processing.[3] This is not only true for perovskite photodetectors, as perovskite solar cells have recently attracted a great deal of interest in the photovoltaic community because of their rapid increase in power conversion efficiency (PCE).[4] Due to the complex geometry of wire-shaped devices, performance in wire-shaped photovoltaic devices lags behind flat substrate devices.[5] This inadequate performance shows a lack in understanding of the fundamental crystallization, fabrication, and engineering of flexible and 3D substrate surfaces.

A trend can be seen in recent wire-shaped photodetectors with the use of ZnO as the light absorbing material, due to its easy fabrication and durability to bending cycles.[5a,6] However, the ZnO-based photodetectors are limited only to the UV region with the best results showing 0.9 A W^{-1} responsivity and 0.28/5.3 s rise/decay time. When following a vertical device structure with multiple layers this complexity adds to both fabrication cost and difficulty.[5a,6] We herein report the development of a carbon-based flexible wire-shaped perovskite photodetector. This flexible wire-shaped device performs exceedingly well under low light environments (11 A W^{-1}) and is easily woven into composites due to its flexibility and small diameter (≈400 µm). Using a novel in-house fabrication method, we have developed a rapid, repeatable, and scalable annealing process to move closer toward the potential of multifunctional composite materials and embedded wire-shaped photodetectors. The photodetector's small size is critical given that any addition to a composite part cannot have a negative impact on its mechanical properties. There has been reported success with integrated wires in composites for structural health monitoring.[7] As these systems use light emissions at 585 and 617 nm, we have characterized our device under the same conditions.

Given the large drop in performance for wire-shaped devices when compared to equivalent structures on planar substrates, fabrication techniques were targeted as a point of improvement; noting that there is no standard method for wire-shaped devices.[8] For comparison, doctor-blade,[9] spray,[10] and spin-coating[11] are all well documented and established fabrication methods for perovskite planar devices. However, wire-shaped cell fabrication exhibits less developed solutions[8a,12] and does not benefit from the history of extensive research found for planar thin film cells. It has been shown that methyl ammonium lead iodide perovskite ($MAPbI_3$) necessitates alternative processing such as two-step deposition or solvent engineering methods to create a pinhole-free, continuous thin film adding additional complexity in the fabrication process.[13] However, using $MAPbI_3$ we have created a continuous thin film on a wire using the joule heating method that shows comparable electrical characteristics to planar rigid perovskite photodetectors.

We have developed a first flexible wire-shaped perovskite photodetector using joule heating method for annealing perovskite on CNY that is repeatable, cost effective, and scalable. This method utilizes joule heating in order to uniformly control the temperature of the wire substrate. We believe we have presented a novel solution able to compete with planar device. To the best of our knowledge, no other publication on a wire-shaped perovskite photodetector on thread-like CNY has

G. R. Adams, Dr. N. Adhikari, H. Parker, Dr. O. Okoli
High Performance Materials Institute
FAMU-FSU College of Engineering
Tallahassee, FL 32310, USA
E-mail: ookoli@fsu.edu

The ORCID identification number(s) for the author(s) of this article can be found under https://doi.org/10.1002/admi.201800082.

DOI: 10.1002/admi.201800082

been reported, which works both as a substrate and charge collector for perovskite photodetector. Equation (1) shows how Joule heating, also known as ohmic or resistive heating, directly converts electric energy to heat (meaning that every joule of electrical energy supplied produces one joule of heat). This is important as it allows for rapid heating or cooling of the substrate, giving a high degree of control to the user

$$Q = I^2\, Rt \tag{1}$$

where Q is heat (joules), I is current (amps), R is resistance (ohms), and t is time (seconds), with DC power supply.

2. Wire-Shaped Perovskite Photodetector Design

Carbon nanotube yarn (CNY) was used as substrate and electron transport layer to prepare perovskite-based wire-shaped photodetector. CNY is comprised of rope spun of four individual carbon nanotube yarn strands which provided sufficient mechanical stability, with thickness resulting in a diameter of ≈400 µm. When making the rope it is critical that the strands hold together during handling and coating, therefore it was found that four CNY strands was the minimum amount to achieve this. The perovskite solution is deposited on the CNY, with indium gallium (Alfa Aesar) as the top electrode. Although gold and silver are often common electrode choices, the indium gallium proved to provide the most consistent contact on the curved surface, while still having a closely matched work function to that of silver.[14]

The fabrication method when using joule heating is illustrated in **Figure 1**. One of the most important features of the CNY threads/wires is their high curvature axial symmetric shape compared to planar substrate. Therefore, it is challenging to control the film uniformity during perovskite layer deposition on CNY along both radial and axial directions. The CNY is placed on a glass slide and connected to a power source for joule heating. In order to ensure complete coverage of perovskite material a slide was designed to raise the CNY up off the glass surface during the annealing process. The quality and thickness of the perovskite film were found to depend on heating current, quantity of the perovskite solution, and number of coating times. The heating current was optimized at ≈0.6 A and ≈2 V (which produced a temperature of 95 °C when measured by the FLIR camera) using 10 µL of perovskite solution per 2 cm CNY yarn to achieve the best film quality, such as adhesion, uniformity, and thickness of the film. Likewise, the hot plate CNY samples were placed on a glass slide and placed on a hot plate at 95 °C. Immediately the solution was added (10 µL per 2 cm of CNY yarn) and the sample was held on the hot plate for 10 min.

3. Results

3.1. Material Characterization

With this new manufacturing technique and using only single-step deposition, we were able to achieve crystalline perovskite

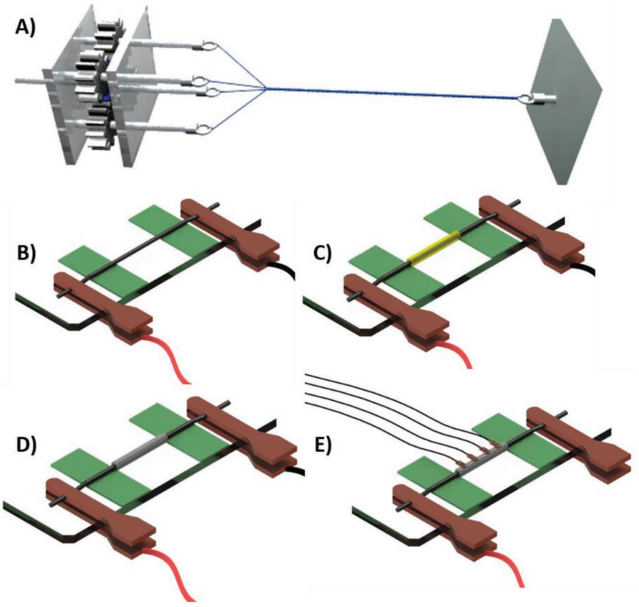

Figure 1. A) Representation of the rope winding mechanism used to create CNY rope. Pitch is defined by a counter which is connected to the geared mechanism. B) Single CNY rope connected to power source for joule heating application. C) Perovskite solution is deposited on the CNY substrate for annealing. D) Annealing yields perovskite crystalline thin film around the body of the CNY device. E) The device is then tested across its length for verification in continuity of crystalline film during characterization.

films comparable to that of flat perovskite photodetector devices.[15] **Figure 2** shows the scanning electron microscope (SEM) results of two types of devices that were fabricated, using joule heating (JH) (Figure 2a,c,e) and hot plate (Figure 2b,d,f) as the heating source for perovskite annealing (SEM images with different magnifications and locations are included in the Supporting Information). Figure 2a shows uniform and compact dense formation of perovskite crystal with size ranging from 0.75 to >2 µm (Figure 2e) by joule heating method. However, nonuniformity, cracks, and some voids were obtained in the perovskite layer prepared using the hot plate method. Although there are large crystalline surfaces (Figure 2b,d,f), it can be seen that there are large pockets where crystal size drops to <100 nm as well as discontinuity of the grains of perovskite. We believe this may be due to the nonuniform distribution of heat applied to the substrate during the annealing process which causes unequal solvent evaporation across the substrate. This results in uncontrolled grain growth of perovskite layer on 3D structure resulting in sharp changes of contrast in SEM images at grain and grain boundary.[16] It is reported that grain boundary in perovskite consists of vacancies, surface defects, and dangling bonds. The origin of these dangling bonds is due to the exposed iodine atoms in the perovskite film.[17] These dangling bonds act as a trap center for electrons and reduces the number of free carriers available for electrical conduction. After trapping the mobile carriers, the traps become electrically charged. This charging generates a potential energy barrier which blocks the motion of carriers from one crystallite to another.

It is also observed that the diameter of perovskite layer prepared by hot plate method is higher than the diameter of

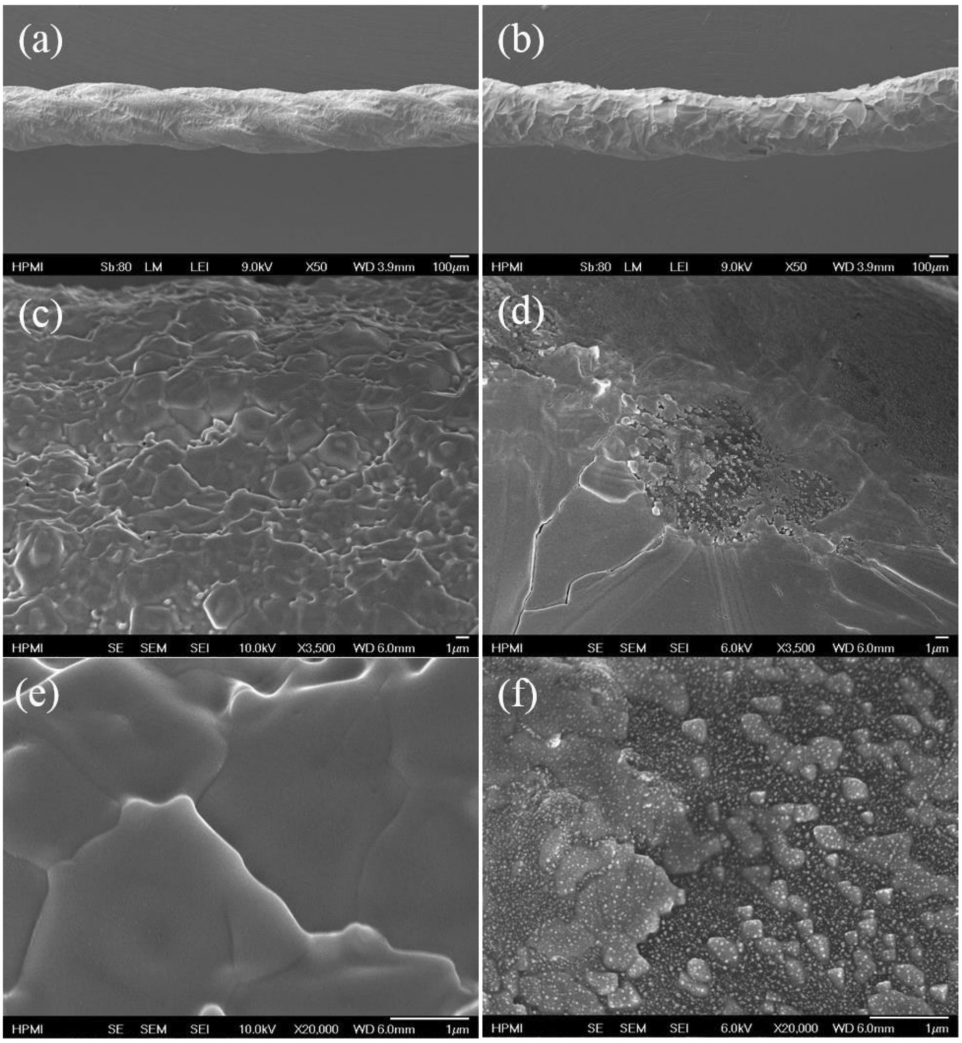

Figure 2. SEM images of $MAPbI_3$ coated CNY using a,c,e) Joule heating and b,d,f) hot plate annealing method at different magnifications.

perovskite layer prepared by joule heating method for the same volume of perovskite solution. This results in poor surface coverage and uncontrolled morphological variations as shown by SEM images (Figure 2b,d,f). The joule heating method provides the uniform temperature throughout the CNY wire for the deposition of the perovskite solution compared to nonuniform temperature obtained through hot plate method as shown from infrared images in Figure S1 (Supporting Information). The uniformity of temperature in case of joule heating technique is due to direct conversion of electrical energy to heat energy applied uniformly on CNY as discussed in Equation (1). It can be seen that nonuniformity in temperature results in pockets of nanocrystals being formed throughout the perovskite layer which occurred in the hot plate heating method (Figures S5 and S6, Supporting Information). These pockets are tiny perovskite crystals in discontinuity with the large film on top. Therefore, the joule heating technique was used to gain a better control of crystal formation and growth mechanism of perovskite crystal on carbon nanotube yarn.

The perovskite crystal structure used for the preparation of wire-shaped photodetector is $CH_3NH_3PbI_3$, where M = CH_3NH_3, A = Pb, and X = I. These crystals are held together by ionic bond between organic and inorganic counterparts and by hydrogen bond.[18] X-ray diffraction (XRD) patterns were recorded to understand the crystallization of perovskite layer on CNY prepared by joule heating and hot plate annealing method. The XRD patterns (Figure S11, Supporting Information) of $MAPbI_3$-coated CNY using joule heating and hot plate annealing method show the Bragg peaks at 14.08° and 28.41° assigned to (110) and (220) plane of $CH_3NH_3PbI_3$. These structures correspond to tetragonal I4cm crystal structure of methyl ammonium lead halide perovskite with high crystallinity.[19] The (110) peak of perovskite phase was highest for samples prepared by joule heating method and also possessed the smaller full width half maximum (FWHM) value of 0.09 indicating greater crystallinity.[20] This shows that the joule heating method results in greater crystallization of perovskite films with preferential grain growth at (110) plane. The surface temperature of the substrate during the film formation affects the degree of surface-induced nucleation because the nucleation events increase with high and uniform temperature throughout the surface.[21] The surface roughness and inhomogeneity of

the CNY wire, as seen in Figure S2 (Supporting Information), allow lower energy pathways for nucleation of the crystallite sites, thus increasing the crystallinity of the perovskite layer on CNY by overcoming the energy barrier for nucleation.[22] The perovskite samples prepared by hot plate method show detectable (110) phase of perovskite as shown in Figure S11 (Supporting Information). However, the intensity is extraordinarily lower in addition to the large amount of noise throughout. Using Gaussian fit, the FWHM value was calculated to be 1.54.

The photoluminescence (PL) spectra (Figure S12, Supporting Information) of perovskite coated on CNY with joule heating method have a high PL intensity at 760 nm compared to perovskite coated on CNY using hot plate. The PL was obtained by exciting the samples by 488 nm light output from a housed 450 W Xe lamp. In order to quantify and compare the PL of the perovskite layer prepared by joule heating and hot plate method, we have calculated the PL efficiency defined as $\rho = I/(P.a)$,[23] where I is the integrated intensity of the PL spectrum, P is the power of the excitation light, and a is the absorption factor at the excitation wavelength (488 nm). The PL efficiency of the perovskite photodetector prepared by joule heating method is ≈2.5 times higher than the PL efficiency of the perovskite photodetector prepared by hot plate method.[23] It is reported that the PL emission depends on the morphologies, crystallinity, grain sizes, and defects[24] in the perovskite film. The PL intensity is high for the perovskite film with large grain size, higher crystallinity, and possesses better optical quality.[25] The PL spectroscopy shown in Figure S12 (Supporting Information) is consistent with the microscopic morphologies and XRD spectroscopy (Figure S11, Supporting Information), which shows largest grain size and highest crystallinity for perovskite layer prepared by joule heating method. The decrease in PL intensity for the hot plate annealed perovskite film can be attributed to higher number of grain boundary area due to small grain sizes. It is found that the grain boundary acts as strong PL quenching site due to nonradiative trap centers.[25,26] The origin of these nonradiative trap centers may be due to the chemical inhomogeneity, presence of defects and dangling bonds.[27] It is reported that the origin of defects and dangling bonds in perovskite film is due to the exposed iodine atoms in the perovskite films.[16]

3.2. Device Characterization

In applications such as embedded sensing,[28] any need for external power adds to both the complexity and cost of the photodetector's implementation; therefore, the device's performance under 0 bias voltage is paramount. The flexible wire-shaped photodetector prepared in this study makes use of asymmetrical electrodes to create the built-in potential without any external bias needed to overcome the binding energy of photogenerated electron–hole pairs.[5a,29] Hybrid perovskite photodetectors have shown very low noise current (I_n) making them a good choice for highly sensitive applications; however, these perovskite photodetector devices are cited to perform best when paired with hole-blocking layers such as poly[(9,9-bis(30-(*N*,*N*-dimethylamino)propyl)-2,7-fluorene)-*alt*-2,7-(9,9-dioctylfluorene)] (PFN).[11d] The devices prepared via hot plate annealing were not studied due to low photocurrent response (Figure S10, Supporting Information) and shorting of the devices due to discontinuity of perovskite absorber layer on the CNY. Due to the pristine crystalline quality, the joule heating samples showed consistent I_n values at 100 pA. This is a huge performance step gained from a technical fabrication procedure, which eliminates the need for further deposition steps and chemicals, minimizing complexity, time, and cost.

Figure 3a shows the *I–V* curves of perovskite photodetector at light and dark conditions. The *I–V* curve of the wire-shaped photodetector shows significant amount of current (≈4.5 nA) without applying any external bias with reproducible signal response as shown in time-dependent photocurrent response (Figure 3b). The photocurrent response is seen to increase with increasing bias voltage as shown in Figure 3c and Figure S9 (Supporting Information). The photocurrent increases more than two times by increasing the voltage level to 2 V with compared to perovskite photodetector device without any external bias voltage. Therefore, the prepared flexible wire-shaped detector is suitable for self-power and low power applications. As bias voltage is linearly changed, a near linear response was obtained from the device as shown in Figure 3d where both the photocurrent and dark current increased predictably. This is due to the change in junction capacitance which decreases allowing for larger current to flow from the device as voltage bias is increased.

The properties of our photodetector to produce a measurable amount of current at zero bias could be contributed to (a) asymmetric work function of the electrodes and (b) changes in the band offsets between CNY/perovskite/In/Ag due to self-passivation of the perovskite layer due to small amount of lead iodide (Figure 3e). The work function of CNY and In/Ag is ≈–4.2[14] and ≈–4.3 eV,[30] and the highest occupied molecular orbital (HOMO) and lowest unoccupied molecular orbital (LUMO) level of perovskite are ≈–5.43 and ≈–3.93 eV.[3] The interface between the CNY and perovskite creates a built-in electric field ($E_b \approx 0.87$ eV) which overcomes the potential barrier and allows the electrons to flow from perovskite to CNY, generating the significant amount of current at zero bias conditions due to photogenerated careers. These carriers are formed due to absorbed photons with energy higher than the energy bandgap of the perovskite materials. The higher value of photocurrent at zero bias may be due to the formation of PbI_2 between the perovskite and CNY, which acts as a hole-blocking layer, reducing the recombination of electron and hole pairs.[16,31] The formation of small amount of lead iodide by single-step method has been widely reported.[16,19b,32] However, the detection of PbI_2 phase in XRD has been limited by the 3D CNY-based substrate resulting in very low signal-to-noise ratio.

Responsivity, the measure of photocurrent per watt of incident light is here described by Equation (2),[11d] where R is responsivity, J_{ph} and J_d are the photocurrent and dark current density, and L_{light} is the incident light power

$$R = \frac{J_{ph} - J_d}{L_{light}} \tag{2}$$

Detectivity (D^*) of the photodetector describes the signal over noise given the incident light. Detectivity is calculated by the responsivity (R) divided by the square root of the dark current

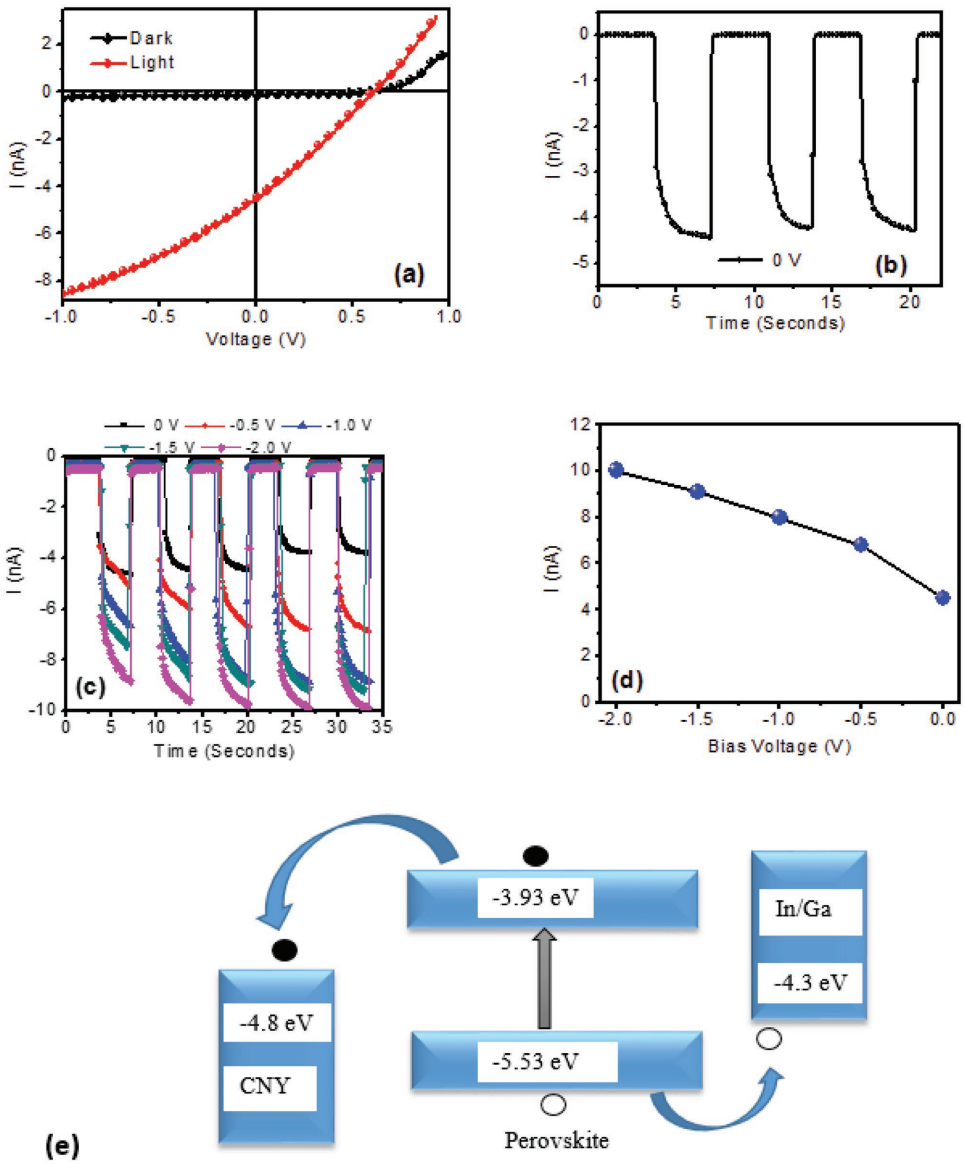

Figure 3. a) Light and dark *I–V* curve of wire-shaped perovskite photodetector with 0 bias. b) Time-dependent photocurrent of wire-shaped perovskite photodetector under 88 W m^{-2} white light for 0 bias. c) Time-dependent photocurrent of wire-shaped perovskite photodetector under 88 W m^{-2} white light for varying bias voltages. d) Effect of bias voltage on the photocurrent response of wire-shaped perovskite photodetector. e) Energy band diagram of wire-shaped perovskite photodetector.

density (J_{dark}). It is critical to suppress dark current as it plays a vital role in the device's ability to sense low light levels. In order to minimize dark current, the light absorbing film must be in pristine condition, minimizing pinholes and trap states within the crystalline structure[11d]

$$D^* = \frac{J_{ph}/L_{light}}{\sqrt{2qJ_{dark}}} \quad (3)$$

The photodetector responsivity (R) and detectivity (D) were calculated using Equations (2) and (3). The incident light (L_{light}) was held constant while the J_{ph} varied as a response to changing bias voltage. In order to calculate J_{ph}, the area was calculated as the diameter of the counter electrode multiplied by the diameter of the CNY/perovskite wire. In **Figure 4**a, the responsivity and detectivity were found to be 330 mA W^{-1} and 5.73×10^9 Jones, respectively, at −2 V bias voltage under white light lamp source with intensity of 8.54 mW cm^{-2}. The prepared CNY/perovskite/In/Ag-based photodetector shows superior responsivity than the photodetector device prepared from multi-wall carbon nanotube thin film (MWCNTF),[33] single-wall carbon nanotube thin film (SWCNTF),[34] single-wall carbon nanotube (SWCNT)/Phenyl-C61-butyric acid methyl ester (PCBM),[35] and single-layer graphene (SLG)-carbon nanotube thin film (CNTF)[36] structures. The response time of the photodetector was calculated using time-dependent photocurrent measurement (Figure 4b). The device shows fast response speed to white light (fast and slow rise time of 132 ms

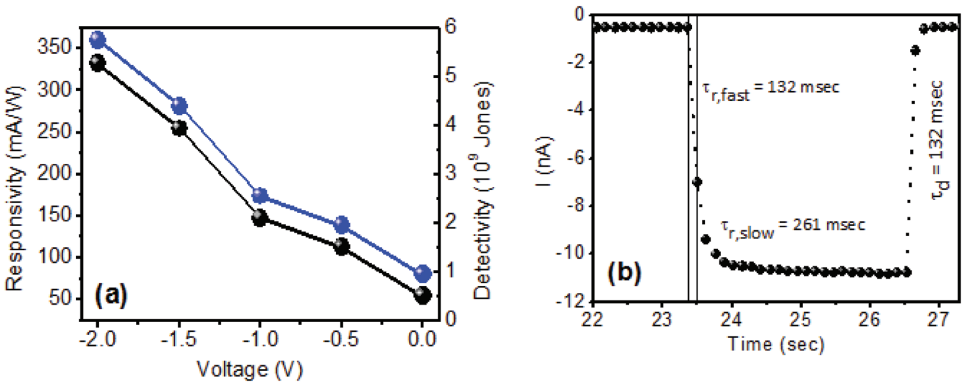

Figure 4. a) Responsivity and detectivity of the wire-shaped perovskite photodetector as a function of bias voltage. b) Rise and fall time of the wire-shaped perovskite photodetector.

and 261 ms, and decay time of 132 ms). The extremely quick decay time indicates a lack of trap states within the crystalline structure, allowing the charges to completely settle to dark current within the measurement confines of the equipment used.

Performance of the wire-shaped device under a varying intensity has shown predictable response through its near linear photocurrent. The wire-shaped device was fixed on an optic table while monochromatic light of 585 and 617 nm wavelength (unfiltered intensity at 0.592 and 0.493 mW, respectively) was directed at the device. Filters (Newport FS-3R Neutral Density Set) at a fixed distance were then placed in the light path in order to vary the light intensities. **Figure 5**a,b shows the linear response to both wavelengths, indicating a strong dependence on incident intensity. The relationship between photocurrent and light intensity was analyzed by fitting with power law: $I_p = CP^\theta$ where C is a constant for the incident light, and the exponent θ determines the sensitivity of photocurrent due to incident light intensity corresponding to 585 and 617 nm ($0.5 < \theta < 1$). The value of θ for 585 and 617 nm incident light was found to be 0.94 and 0.98. Such a high value of θ suggests a low density of trap states in the CNY/perovskite/In/Ag photodetector.

The responsivity and detectivity of the photodetector were studied with low light intensity from 0 to ≈0.9 mW cm^{-2} to further understand the light intensity dependent photoresponse. As shown in Figure 5c, the responsivity and detectivity increase gradually with decreasing intensity. However, the responsivity and detectivity saturate with further increase of the intensity due to reduced charge carrier recombination rate at higher light intensity. Furthermore, the device was tested for photoresponse under varying wavelength (Figure S7, Supporting Information) showing a response from 350 to 800 nm, corresponding to the PL measurements seen in Figure S12 (Supporting Information).

In creating a flexible carbon device, it is the ultimate goal to embed these devices into carbon fiber composites, creating a way forward for multifunctional composites and in situ structural health monitoring (SHM). To test weavability, the devices were clipped onto 3D-printed curves in order to hold the specimen in shape and simulate its woven environment. The mechanical stability of the photodetectors was studied with structures having radii of curvatures: 0 mm^{-1} (flat), 0.1 mm^{-1}, and 0.25 mm^{-1} as shown in **Figure 6**. Time-dependent photocurrent response was measured as a function of strain. The comparable photocurrent was obtained while increasing the strain for curvatures from flat to 0.25 mm^{-1}. There is a slight decrease in photocurrent as the bending radius is decreased. We believe what we are seeing here is a combination of the effect of curvature on the crystalline perovskite structure around the device and the change in active area. Given that the light source is focused directly above the device, the active area diminishes as the device is further

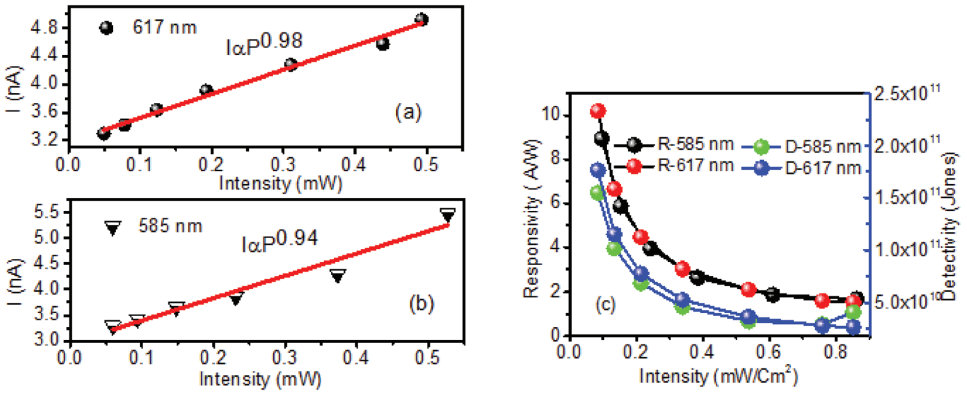

Figure 5. Photocurrent dependence of wire-shaped perovskite photodetector with varying light intensity at 0 V: a) 617 and b) 585 nm. c) Responsivity and detectivity of wire-shaped perovskite photodetector at 585 and 617 nm wavelength.

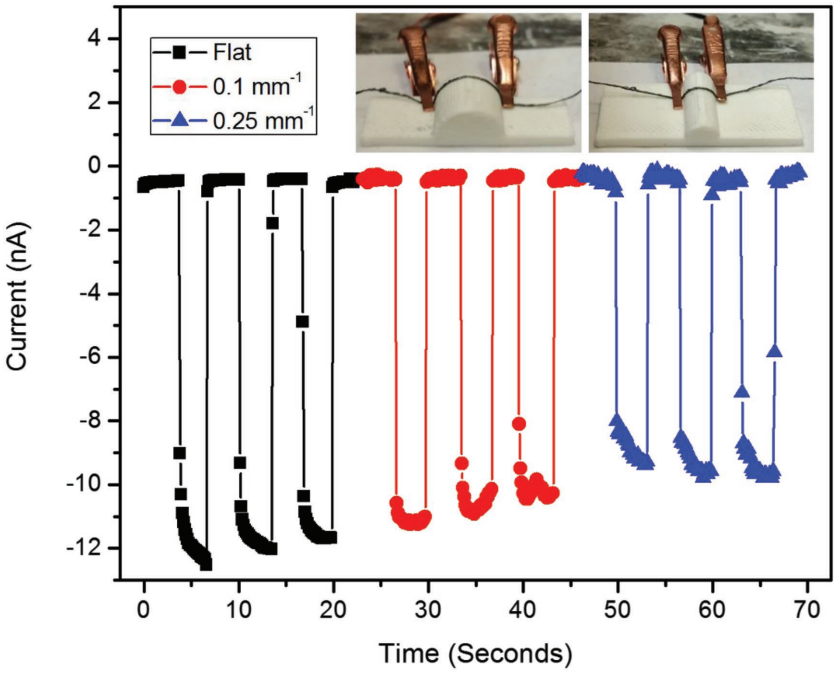

Figure 6. Time-dependent current responses of wire-shaped perovskite photodetector with flat, 0.1 and 0.25 mm^{-1} radii of curvatures. Photo inlays show how the device was held during testing.

bent. This slight decrease in performance as the device is bent has been a problem among other devices as well.[37] Furthermore, the device retained its linear photocurrent response to varying bias voltage while under bending conditions (Figure S8, Supporting Information).

The overall performance of this single-step solution $MAPbI_3$ device is remarkable. When looking at the performance of our device in comparison to wire-shaped, flexible planar, and rigid planar devices in **Table 1**, it shows a very comparable responsivity, I_{light}/I_{dark} ratio, and response time. Noting that the complex 3D surface of wire-shaped devices presents challenges during fabrication, we believe we have presented a solution able to compete with planar devices. During this review no other publication of a wire-shaped perovskite photodetector could be found. Although there are some publications of perovskite solar devices, we believe this is the first wire-shaped perovskite photodetector reported.

Table 1. Performance summary of wire-shaped, flexible planar, and rigid planar photodetectors, with a focus on perovskite-based devices.

Device	Bias [V]	Responsivity [A W^{-1}]	I_{light}/I_{dark}	Response time [s]	Type
Our device	0	10.2	45	0.393/0.132	Wire-shaped
ZnO[38]	1	–	4	7.5/8.6	Wire-shaped
NiO/ZnO[6a]	–3.5	21.8	4.9	–/18.1	Wire-shaped
ZnO[5a]	0	0.00996	2	1.5/6	Wire-shaped
ZnO[6b]	–0.5	0.9	7.2	0.28/2.2	Wire-shaped
Perovskite[39]	0	115	–	0.25/5.3	Flexible planar
Perovskite[37b]	0.6	0.101	29	<0.2	Flexible cloth
Perovskite/ZnO[40]	0	24.3	–	0.7/0.6	Planar
MWCNT[33]	–	–	–	0.001	Planar
SWCNT[34]	–	9.87×10^{-5}	–	–	Planar
SWCNT/PCBM[35]	–0.6	0.26	–	–	Planar
SLG-CNTF	–	0.209	100	$6.8 \times 10^{-5}/7.8 \times 10^{-5}$	Planar

4. Conclusion

We have developed a flexible wire-shaped perovskite photodetector using joule heating method. By uniformly controlling the substrate temperature we were able to create pristine crystalline films of perovskite on CNY wires. The perovskite ($MAPbI_3$) photodetector prepared by single-step method shows strong responsivity (10.2 A W^{-1}), detectivity (1.76×10^{11} J), and I_{light}/I_{dark} (45) with 0 V bias. The device shows good flexibility with sustainable photocurrent under varying bending angles. It is found that uniform heat is necessary for the crystallization of the absorber layer on the CNY substrate. When a constant temperature is applied across the substrate region, evaporation of the solvent occurs evenly, allowing for a thin and uniform film to form over the CNY. This gives great promise moving forward to apply more advanced perovskite solution chemistries with this technique in order to minimize the performance gap between flat and wire-shaped perovskite photovoltaic devices.

5. Experimental Section

Perovskite Synthesis: The perovskite layer was prepared using a single-step deposition method. The solution was prepared inside the glove box in a controlled atmosphere. First, methylammonium iodide (CH_3NH_3I; Sigma Aldrich) was weighed out to 113 mg (710×10^{-6} M). Next, 710 µL of γ-butyrolactone (GBL; Sigma Aldrich) was added to the CH_3NH_3I and stirred for 5 min at 50 °C in order to create a 1:1 molar ratio solution. Next, 187 mg of lead iodide (PbI_2; Sigma Aldrich) was weighed out in a separate container. The CH_3NH_3I/GBL solution was added to the PbI_2 powder and stirred at 65 °C for 40 min to create a 1.75 M:1 M (CH_3NH_3I:PbI_2) perovskite solution.

Materials and Device Characterization: The crystalline structure of the as-prepared materials was characterized by powder X-ray diffraction (Scintag XRD Powder Diffractometer). Steady-state emission data were collected at room temperature using an Edinburgh FLS980 spectrometer. Samples were excited by light output from a housed 450 W Xe lamp passing through a single grating (1800 l mm^{-1}, 250 nm blaze) Czerny-Turner monochromator, and finally a 5 nm bandwidth slit. Emission from the sample was passed through a 570 nm long pass filter, a single grating (1800 l mm^{-1}, 500 nm blaze) Czerny-Turner monochromator (21 nm bandwidth),

and thus detected by a peltier-cooled Hamamatsu R928 photomultiplier tube. SEM images were taken by a high-resolution field emission scanning electron microscope (FESEM) (JEOL 7401F). The *I–V* (current–voltage) and *I–t* (current–time) measurements of the flexible wire-shaped photodetector were obtained by a Keithley 2400 integrated with Labview. The perovskite photodetectors were tested using white light, 585 and 617 nm LED.

Supporting Information

Supporting Information is available from the Wiley Online Library or from the author.

Acknowledgements

The authors thank Tristan Dilbeck (FSU Chemistry Department) for performing the PL measurements and Dr. Hanson for allowing to use his lab equipment which was used to perform the PL and light intensity measurements. Finally, the authors thank Haoran (Clark) Li (FSU Industrial Engineering Department) for performing some of the XRD measurements. The funding for this work was provided by the NSF Award Nos. 1359235 and NSF/DMR-1644779.

Conflict of Interest

The authors declare no conflict of interest.

Keywords

flexible, joule heating, perovskite, photodetector, wire-shaped

Received: January 16, 2018
Revised: March 2, 2018
Published online: May 21, 2018

[1] a) G. Weckler, *IEEE Int. Electron Devices Meet.*, **1965**; b) A. E. Becquerel, Mémoire sur les effets électriques produits sous l'influence des rayons solaire, Comptes Rendus, Originalarbeit zur Einwirkung von Licht auf Elektroden 9 **1839**, 561–567.

[2] a) V. Sukhovatkin, S. Hinds, L. Brzozowski, E. H. Sargent, *Science* **2009**, *324*, 1542; b) P. Schilinsky, C. Waldauf, J. Hauch, C. J. Brabec, *Thin Solid Films* **2004**, *451*, 105; c) Y. Jin, J. Wang, B. Sun, J. C. Blakesley, N. C. Greenham, *Nano Lett.* **2008**, *8*, 1649; d) H. Haugan, S. Elhamri, F. Szmulowicz, B. Ullrich, G. Brown, W. Mitchel, *Appl. Phys. Lett.* **2008**, *92*, 071102; e) X. Gan, R.-J. Shiue, Y. Gao, I. Meric, T. F. Heinz, K. Shepard, J. Hone, S. Assefa, D. Englund, *Nat. Photonics* **2013**, *7*, 883; f) F. Binet, J. Duboz, E. Rosencher, F. Scholz, V. Härle, *Appl. Phys. Lett.* **1996**, *69*, 1202.

[3] Z. Song, S. C. Watthage, A. B. Phillips, M. J. Heben, *J. Photonics Energy* **2016**, *6*, 022001.

[4] X. Zhang, H. Lin, H. Huang, C. Reckmeier, Y. Zhang, W. C. Choy, A. L. Rogach, *Nano Lett.* **2016**, *16*, 1415.

[5] a) Y. Dong, Y. Zou, J. Song, Z. Zhu, J. Li, H. Zeng, *Nano Energy* **2016**, *30*, 173; b) M. Lee, Y. Ko, Y. Jun, *J. Mater. Chem. A* **2015**, *3*, 19310; c) NREL, Energy Technology Cost and Performance Data for Distributed Generation, http://www.nrel.gov/analysis/tech_footprint.html (accessed: December 2017).

[6] a) Y. H. Ko, G. Nagaraju, J. S. Yu, *Nanoscale* **2015**, *7*, 2735; b) Z. Zhu, D. Ju, Y. Zou, Y. Dong, L. Luo, T. Zhang, D. Shan, H. Zeng, *ACS Appl. Mater. Interfaces* **2017**, *9*, 12092.

[7] a) D. O. Olawale, J. Yan, D. H. Bhakta, D. Carey, T. J. Dickens, O. I. Okoli, *Mechanics of Composite and Multi-functional Materials*, Vol. *7*, Springer, Berlin **2016**, p. 55; b) D. O. Olawale, T. Dickens, W. G. Sullivan, O. I. Okoli, J. O. Sobanjo, B. Wang, *J. Lumin.* **2011**, *131*, 1407; c) T. J. Dickens, O. I. Okoli, *J. Reinf. Plast. Compos.* **2011**, *30*, 1869.

[8] a) R. Li, X. Xiang, X. Tong, J. Zou, Q. Li, *Adv. Mater.* **2015**, *27*, 3831; b) M. Peng, D. Zou, *J. Mater. Chem. A* **2015**, *3*, 20435.

[9] a) S. Tang, Y. Deng, X. Zheng, Y. Bai, Y. Fang, Q. Dong, H. Wei, J. Huang, *Adv. Energy Mater.* **2017**, *7*, 1700302; b) Y. Deng, E. Peng, Y. Shao, Z. Xiao, Q. Dong, J. Huang, *Energy Environ. Sci.* **2015**, *8*, 1544.

[10] a) A. T. Barrows, A. J. Pearson, C. K. Kwak, A. D. Dunbar, A. R. Buckley, D. G. Lidzey, *Energy Environ. Sci.* **2014**, *7*, 2944; b) G. Chai, S. Wang, Z. Xia, S. Luo, C. Teng, T. Yang, Z. Nie, T. Meng, H. Zhou, *Semicond. Sci. Technol.* **2017**, *32*, 074003.

[11] a) L. Tzounis, T. Stergiopoulos, A. Zachariadis, C. Gravalidis, A. Laskarakis, S. Logothetidis, *Mater. Today: Proc.* **2017**, *4*, 5082; b) D.-h. Song, J. H. Heo, H. J. Han, M. S. You, S. H. Im, *J. Power Sources* **2016**, *310*, 130; c) N. J. Jeon, J. H. Noh, Y. C. Kim, W. S. Yang, S. Ryu, S. I. Seok, *Nat. Mater.* **2014**, *13*, 897; d) L. Dou, Y. M. Yang, J. You, Z. Hong, W.-H. Chang, G. Li, Y. Yang, *Nat. Commun.* **2014**, *5*, 5404.

[12] S. He, L. Qiu, X. Fang, G. Guan, P. Chen, Z. Zhang, H. Peng, *J. Mater. Chem. A* **2015**, *3*, 9406.

[13] a) N. Adhikari, A. Dubey, E. A. Gaml, B. Vaagensmith, K. M. Reza, S. A. A. Mabrouk, S. Gu, J. Zai, X. Qian, Q. Qiao, *Nanoscale* **2016**, *8*, 2693; b) M. Grätzel, *Nat. Mater.* **2014**, *13*, 838.

[14] R. C. Chiechi, E. A. Weiss, M. D. Dickey, G. M. Whitesides, *Angew. Chem.* **2008**, *120*, 148.

[15] a) Q. Wang, Y. Shao, Q. Dong, Z. Xiao, Y. Yuan, J. Huang, *Energy Environ. Sci.* **2014**, *7*, 2359; b) G. E. Eperon, V. M. Burlakov, P. Docampo, A. Goriely, H. J. Snaith, *Adv. Funct. Mater.* **2014**, *24*, 151.

[16] N. Adhikari, A. Dubey, D. Khatiwada, A. F. Mitul, Q. Wang, S. Venkatesan, A. Iefanova, J. Zai, X. Qian, M. Kumar, *ACS Appl. Mater. Interfaces* **2015**, *7*, 26445.

[17] N. Adhikari, A. Dubey, E. Gaml, B. Vaagensmith, K. Reza, S. mabrouk, S. Gu, J. Zai, X. Qian, Q. Qiao, *Nanoscale* **2015**, *8*, 2693.

[18] a) S. Venkatesan, E. C. Ngo, Q. Chen, A. Dubey, L. Mohammad, N. Adhikari, A. F. Mitul, Q. Qiao, *Nanoscale* **2014**, *6*, 7093; b) T. Glatzel, D. F. Marrón, T. Schedel-Niedrig, S. Sadewasser, M. C. Lux-Steiner, *Appl. Phys. Lett.* **2002**, *81*, 2017.

[19] a) S. Venkatesan, N. Adhikari, J. Chen, E. C. Ngo, A. Dubey, D. W. Galipeau, Q. Qiao, *Nanoscale* **2014**, *6*, 1011; b) J. S. Yun, A. Ho-Baillie, S. Huang, S. H. Woo, Y. Heo, J. Seidel, F. Huang, Y.-B. Cheng, M. A. Green, *J. Phys. Chem. Lett.* **2015**, *6*, 875.

[20] C. Sun, Y. Guo, B. Fang, L. Guan, H. Duan, Y. Chen, H. Li, H. Liu, *RSC Adv.* **2017**, *7*, 22492.

[21] Y. Tidhar, E. Edri, H. Weissman, D. Zohar, G. Hodes, D. Cahen, B. Rybtchinski, S. Kirmayer, *J. Am. Chem. Soc.* **2014**, *136*, 13249.

[22] J. Dirksen, T. Ring, *Chem. Eng. Sci.* **1991**, *46*, 2389.

[23] S. Zhang, P. Audebert, Y. Wei, A. Al Choueiry, G. Lanty, A. Bréhier, L. Galmiche, G. Clavier, C. Boissiere, J.-S. Lauret, *Materials* **2010**, *3*, 3385.

[24] A. Al Mamun, T. T. Ava, H. J. Jeong, M. S. Jeong, G. Namkoong, *Phys. Chem. Chem. Phys.* **2017**, *19*, 9143.

[25] G. Namkoong, H. J. Jeong, A. Mamun, H. Byun, D. Demuth, M. S. Jeong, *Sol. Energy Mater. Sol. Cells* **2016**, *155*, 134.

[26] W. Zhang, S. Pathak, N. Sakai, T. Stergiopoulos, P. K. Nayak, N. K. Noel, A. A. Haghighirad, V. M. Burlakov, A. Sadhanala, W. Li, *Nat. Commun.* **2015**, *6*, 10030.

[27] P. Cui, P. Fu, D. Wei, M. Li, D. Song, X. Yue, Y. Li, Z. Zhang, Y. Li, J. M. Mbengue, *RSC Adv.* **2015**, *5*, 75622.
[28] J. Yan, M. J. Uddin, D. O. Olawale, T. J. Dickens, O. O. Okoli, *Triboluminescence*, Springer, Berlin **2016**, p. 351.
[29] D. Xiang, C. Han, Z. Hu, B. Lei, Y. Liu, L. Wang, W. P. Hu, W. Chen, *Small* **2015**, *11*, 4829.
[30] H. B. Michaelson, *J. Appl. Phys.* **1977**, *48*, 4729.
[31] Q. Chen, H. Zhou, T.-B. Song, S. Luo, Z. Hong, H.-S. Duan, L. Dou, Y. Liu, Y. Yang, *Nano Lett.* **2014**, *14*, 4158.
[32] a) C.-S. Jiang, M. Yang, Y. Zhou, B. To, S. U. Nanayakkara, J. M. Luther, W. Zhou, J. J. Berry, J. van de Lagemaat, N. P. Padture, *Nat. Commun.* **2015**, *6*, 8397; b) A. Dymshits, A. Henning, G. Segev, Y. Rosenwaks, L. Etgar, *Sci. Rep.* **2015**, *5*, 8704.
[33] R. Lu, J. J. Shi, F. J. Baca, J. Z. Wu, *J. Appl. Phys.* **2010**, *108*, 084305.
[34] Q. Zeng, S. Wang, L. Yang, Z. Wang, T. Pei, Z. Zhang, L.-M. Peng, W. Zhou, J. Liu, W. Zhou, *Opt. Mater. Express* **2012**, *2*, 839.
[35] Y. Xie, M. Gong, T. A. Shastry, J. Lohrman, M. C. Hersam, S. Ren, *Adv. Mater.* **2013**, *25*, 3433.
[36] T.-F. Zhang, Z.-P. Li, J.-Z. Wang, W.-Y. Kong, G.-A. Wu, Y.-Z. Zheng, Y.-W. Zhao, E.-X. Yao, N.-X. Zhuang, L.-B. Luo, *Sci. Rep.* **2016**, *6*, 38569.
[37] a) S. Chen, C. Teng, M. Zhang, Y. Li, D. Xie, G. Shi, *Adv. Mater.* **2016**, *28*, 5969; b) H. Sun, T. Lei, W. Tian, F. Cao, J. Xiong, L. Li, *Small* **2017**.
[38] J. Chen, L. Ding, X. Zhang, L. Chu, N. Liu, Y. Gao, *Opt. Express* **2014**, *22*, 3661.
[39] V. Q. Dang, G.-S. Han, T. Q. Trung, Y.-U. Jin, B.-U. Hwang, H.-S. Jung, N.-E. Lee, *Carbon* **2016**, *105*, 353.
[40] J. Yu, X. Chen, Y. Wang, H. Zhou, M. Xue, Y. Xu, Z. Li, C. Ye, J. Zhang, P. A. Van Aken, *J. Mater. Chem. C* **2016**, *4*, 7302.

